Received: 11 May 2020 | Revised: 16 November 2020 | Accepted: 25 November 2020

IET Microwaves, Antennas & Propagation

DOI: 10.1049/mia2.12082

The Institution of Engineering and Technology WILEY

ORIGINAL RESEARCH PAPER

Angular characteristics of multipath propagation in an indoor industrial environment

Aliou Bamba[1,2] | Emmeric Tanghe[2] | Aladji Kamagaté[1,3] | Pierre Laly[4] | Frédéric Challita[4] | Adama Konaté[1] | Wout Joseph[2] | Martine Liénard[4] | Davy P. Gaillot[4]

[1]Direction de la Recherche et de l'Innovation Technologique – Ecole Superieure Africaine des TIC Blvd Marseille, Abidjan, Cote d'Ivoire

[2]Department of Information Technology Ghent University – iMEC, Wireless, Acoustics, Environment & Expert Systems, Ghent, Belgium

[3]Département Numérique et Mathématiques (NuMa), Agence Nationale de la Recherche, Paris, France

[4]Institut d'Electronique, de Microélectronique, et de Nanotechnologie, Université de Lille, Villeneuve d'Ascq, France

Correspondence

Aliou Bamba, Direction de la Recherche et de l'Innovation Technologique – Ecole Superieure Africaine des TIC Blvd Marseille, Abidjan, Treichville, Km4 Bd de Marseille - 18 BP 1501 Abidjan 18.
Email: aliou.bamba@esatic.edu.ci

Abstract

The characteristics of multipath components (MPCs) are addressed in an industrial environment at 1.3 GHz by means of measurements with a multidimensional channel sounder. The maximum likelihood estimator, RiMAX, is used to determine the MPCs parameters and takes into account the diffuse scattering. Both line-of-sight (LOS) and obstructed LOS (OLOS) scenarios have been considered, along with the four polarization states. We found that the environment is very rich in multipath, that is on average, about 120 (resp. 70) MPCs in LOS (resp. OLOS) scenario due to the presence of several metallic reflectors. The azimuthal angle implies clustering of the MPCs, and therefore, the estimated MPCs are grouped in clusters using the *K*-powers-means algorithm based on the multipath component distance. In general, one to four clusters are determined with three clusters occurring with the highest probability, regardless of the scenario. Next, the intra-cluster parameters have been determined, and we show that the root-mean-square (rms) delay spread and rms angular spread follow a gamma distribution, regardless of the polarization. The MPC characteristics agree with the results in the literature and can be valuable when deploying a wireless sensor network in industrial environments.

1 | INTRODUCTION

Potential benefits of the wireless sensors networks (WSNs) for the industrial companies have been evidenced for decades [1–4]. However, companies are reluctant in the deployment of the WSN, despite its potentials as a lack of reliability or an outage which may cause severe damage to their materials, workers, and finances.

Currently, it is expected that the 5th generation (5G) of mobile communications systems will allow an infinite number of applications, as all of its capabilities and potentials are not yet identified until now. One of the use cases of the 5G—namely the massive Machine-Type Communications—corresponds to scenarios with a massive number of devices having a very long battery life [5]. Another use case is the ultra-reliable and low-latency critical communications where stringent requirements for capabilities such as high data rates, very low latency, and availability will be satisfied. As a consequence, it is expected that these scenarios will be largely used in industrial manufacturing for efficient and reliable automation and safety purposes. Depending on the applications and the associated requirements, the future 5G will operate at lower frequencies, for example below 6 GHz [5, 6]. Especially, this will be the case for manufacturing industries where massive internet of things (IoTs) devices or networks will be deployed for automation and safety purposes.

Channel modelling and characterization in industrial environments is an important step for the WSN deployments [7, 8]. Indeed, before the deployment of an IoT network in such environments, the propagation mechanisms and characteristics must be well determined and understood to optimize the network performance in terms of data rates, availability, reliability, and so on.

Using an electromagnetic analysis software, ref. [9] predicted the electric field attenuation and the phase variation as a function of the frequency in three industrial sites. Measurement-based

large-scale parameters have been determined in different classes of industrial environments [10], in open production space and dense factory clutter at 2.3 GHz and 5.7 GHz [11]. Three ultra-wide-band measurement campaigns were conducted in the frequency range of 3.1–5.5 GHz and 3.1–10.6 GHz in two different industrial environments [12], wherein the presence of dense multipath components (DMCs) has been evidenced, especially due to the abundance of metallic structures. Moreover, [12–15] show that the multipath components (MPCs) arrive in cluster in industrial environments and the radio channel can be consequently modelled according to the Saleh–Valenzuela [16] model.

An analysis of the polarization characteristics of specular and DMC in a large industrial hall is performed at 1.3 GHz within 22 MHz bandwidth [17]. The study investigated the co-polar and cross-polar DMC power as well as the cross-polar discrimination (XPD) and co-polar ratio (CPR).

Furthermore, the use of directive antennas in indoor environments can significantly increase the signal gain and also decrease the interference level, improving thereby the overall system performances [18, 19], such as the throughput enhancement, delay reduction, and so on. However, the effective directionality of a system depends not only on the antenna system, but also on the considered environment [20]. Hence, the directions of arrival of the MPCs have been investigated in various indoor environments [21–29]. The cross-polarized signals exhibit similar power levels for all elevation angles, while co-polarized signals appear in clusters in the azimuthal plane [21]. It is also shown that the co-polarized signals are more spread in the azimuthal plane, whereas the cross-polarized ones are concentrated in few directions [21, 22]. This observation is further confirmed by experiments at 60 GHz in a conference room at 60 GHz [24], in two office rooms in the V- and E-bands [27], in several indoor environments at 28 GHz [28] and in the D-band [29] where it turns out that the MPCs are spread over the entire azimuthal plane, that is, $[0, 2\pi)$. Besides, the MPCs are more spread in the non line-of-sight (NLOS) conditions than in the LOS [25]. The variation of the angular spreads as a function of the distance between transceiver is experimentally investigated at 72 GHz in an indoor hall, and it is found that the directional dispersion of indoor channels is more sparse than those obtained at lower frequencies [23]. Based on a measurement campaign carried out in an indoor office from 6 to 60 GHz, ref. [26] has shown that the measured channel power distributions over direction and delay are similar over the full frequency range in both LOS and NLOS scenarios.

However, industrial environments are a special case of indoor environments as they are usually larger and are comprised of more reflectors and/or obstacles. As a consequence, compared to other indoor environments, industrial environments are richer in MPCs and these MPCs are more diffuse as they stem from various and broader directions. These differences impact the channel characteristics, and eventually, the performances of a system deployed in such environments. For instance, two different indoor environments have been characterized in [14], and it has been shown that the technologies based on multi-functional antennas can give increased performance in highly reflective environments, whereas no improvement is gained in highly absorbent environments. Indeed, the reflections from various objects in an industrial environment can be a reason for a good coverage experience in the presence of the LOS or NLOS conditions. Additionally, the channel impulse response, delay spread, coherence bandwidth, and so on have been experimentally investigated at 2.4 GHz [30], and it is observed that these characteristics do not depend mainly on LOS conditions, but are rather associated to heavy obstruction configurations in the investigated industrial environment.

To the best of our knowledge, very few studies have investigated the MPCs' angular characteristics in industrial environments. Notwithstanding, ref. [31] derived an analytical expression of the pdf of the angle-of-arrival (AoA) and a geometry-based channel model determined analytical expressions of the probability density functions of channel parameters such as the AoA, time-of-arrival to model wide-band channel in industrial indoor environments [20].

The present study aims at filling this gap, that is, characterization of the MPCs—in the angular domain—in an industrial environment. The novelties of our studies are (i) the characterization of the multipath in the angular domain, (ii) the clustering of the multipath, and (iii) the assessment of intra-cluster large scale parameters and their properties.

The study is organized as follows. Section 2 shortly describes the considered environment, the equipments, and the data collection method. Section 3 presents the data processing methodology, and Section 4 presents and analyzes the results. Finally, Section 5 concludes the study.

2 | MEASURED ENVIRONMENT AND DATA COLLECTION

2.1 | Measured environment

The investigated industrial environment is the same used in [17]. It is a large hall located in Zwijnaarde, Belgium. The hall dimensions are $21.3 \times 77.2 \times 12.2\ m^3$. The inventory is a dense indoor environment comprised of several obstacles such as metallic machinery, concrete structure, large tables or desks, storage cabinets, robots and so on. It mainly consists of large metallic machinery used to test the robustness of small to large concrete structures. The dominant building material for walls, floor, and ceiling is concrete. The windows are located near the ceiling, and a large metallic industrial door is located at one end of the hall and closes it [17]. Figure 1 illustrates a view of the investigated environment. The Tx and the Rx were static in their respective locations during the measurement. Once the measurement in that configuration was completed, the Tx was moved in another location, and the measurement was carried out in a static position of both the Tx and Rx. This process was repeated for 26 locations of the Tx and 3 locations of the Rx in either LOS or OLOS, as illustrated in Figure 1(b).

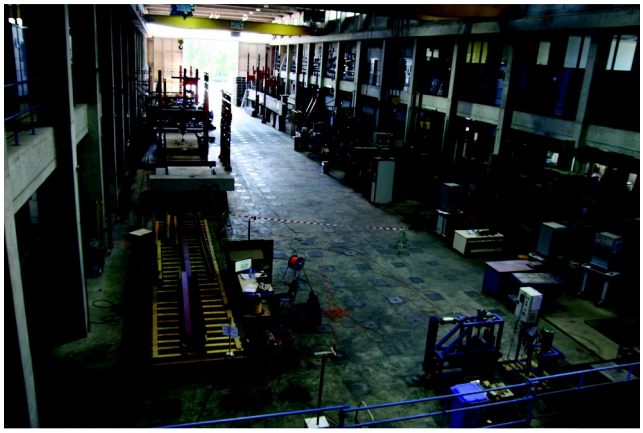

(a) Overview of the interior of the industrial environment

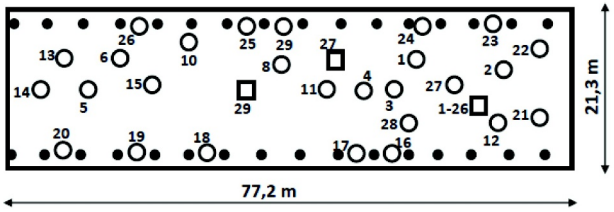

(b) Floor plan of the industrial hall. The black circles indicates the position of the tall concrete supports at each side of the hall. The circles and squares designate the Tx and Rx positions, respectively.

FIGURE 1 Industrial environment

Furthermore, all the measurements were performed in static scenario, and no machine was running.

2.2 | Data collection

We use the data measurements from [17] for our study. A summary of the measurement procedure is as follows. The environment has been probed with a multidimensional channel sounder. An Agilent E5071C—4-port vector network analyzer (VNA)—was used to measure the full polarimetric radio channel. The central frequency was set to 1.3 GHz within a bandwidth of 22 MHz uniformly spaced into $M_f = 1601$ frequency points. A virtual antenna array was created by mounting an antenna on an automated rotating arm. The antenna element used for the measurement is described in [17]. At both the Tx and Rx side, dual-polarized patch antennas were used. The Tx and Rx antennas were mounted at 1.60 m above the ground level. The virtual array was a planar horizontal uniform circular array (UCA) with radius of 15 cm and consisting of $M_T = M_R = 12$ antenna elements. M_T (resp. M_R) is the number of antenna elements at the Tx (resp. Rx) side. The 4-port VNA measures the vertical (V) and horizontal (H) components at the Rx simultaneously. The antennas have at least 15 dB XPD with 120° and 100° half-power beamwidth measured respectively in the azimuth and elevation plane. The measured co- and cross-polar far-field radiating patterns of the antenna for the V and H ports at 1.3 GHz can be seen in the figure 2 of [17]. Further details on the measurement procedure and the used antennas can be found in [17].

3 | DATA PRE-PROCESSING METHODOLOGY

3.1 | Specular multipath estimation

The full polarimetric channel matrix is given by:

$$\mathbf{H} = \begin{pmatrix} \mathbf{h}_{\mathrm{HH}} & \mathbf{h}_{\mathrm{HV}} \\ \mathbf{h}_{\mathrm{VH}} & \mathbf{h}_{\mathrm{VV}} \end{pmatrix} \tag{1}$$

where $\mathbf{h}_{\mathrm{XY}} \in \mathbb{C}^{M_T M_R M_f \times 1}$ is the measured radio channel in the frequency domain. The subscripts X and Y denote the polarization of the Tx and Rx antenna, respectively. X and Y are either H or V.

The wireless narrow band radio channel $\mathbf{h}_{\mathrm{XY}}$ can be considered as a superposition of deterministic specular multipath components (SMCs) $s(\Theta_{\mathrm{smc}}^{\mathrm{XY}})$ and stochastic DMC $d(\Theta_{\mathrm{dmc}})$ including diffuse components [32, 33] and noise. $s(\Theta_{\mathrm{smc}}^{\mathrm{XY}})$ and $d(\Theta_{\mathrm{dmc}})$ are the set of parameters that fully describe the propagation mechanisms:

$$\mathbf{h}_{\mathrm{XY}} = \mathbf{s}(\Theta_{\mathrm{smc}}^{\mathrm{XY}}) + \mathbf{d}(\Theta_{\mathrm{dmc}}) + \mathbf{n} \tag{2}$$

where $\mathbf{h}_{\mathrm{XY}}$, $\mathbf{s}(\Theta_{\mathrm{smc}}^{\mathrm{XY}}) \in \mathbb{C}^{M_T M_R M_f \times 1}$, $\mathbf{d}(\Theta_{\mathrm{dmc}}) \in \mathbb{C}^{M_T M_R M_f \times 1}$, and $\mathbf{n} \in \mathbb{C}^{M_T M_R M_f \times 1}$ are the sampled version of an observation of the channel, the contribution of the SMC, the contribution of the DMC, and the additive measurement noise. The contribution $\mathbf{s}(\Theta_{\mathrm{smc}}^{\mathrm{XY}})$ is deterministic, whereas the contributions $\mathbf{d}(\Theta_{\mathrm{dmc}})$ and $\mathbf{n}$ are both realization of an independent and identically distributed (i.i.d) circular complex normal distributed process expressed respectively by Equations (3) and (4).

$$\mathbf{d}(\Theta_{\mathrm{dmc}}) \sim \mathcal{N}_c(0, \mathbf{R}(\Theta_{\mathrm{dmc}})) \tag{3}$$

where $\mathcal{N}_c(m, \mathbf{R})$ designates a complex circular symmetric Gaussian process with mean m and covariance matrix $\mathbf{R}$.

$$\mathbf{n} \sim \mathcal{N}_c(0, \sigma_n^2 \mathbf{I}) \tag{4}$$

where σ_n^2 and $\mathbf{I}$ are the noise variance, and the identity matrix of size $M \times M$ with $M = M_T \times M_R \times M_f$.

In light of the aforementioned statements, a channel observation is then distributed according to Equations (5).

$$\mathbf{h}_{\mathrm{XY}} \sim \mathcal{N}_c\left(\mathbf{s}(\Theta_{\mathrm{smc}}^{\mathrm{XY}}), \mathbf{R}(\Theta_{\mathrm{dmc}}) + \sigma_n^2 \mathbf{I}\right) \tag{5}$$

The diffuse parameter vector is defined as:

$$\Theta_{\mathrm{dmc}} = [\tau_d \quad \alpha_1 \quad \beta_d] \tag{6}$$

where τ_d, α_1, and β_d are the normalized base arrival delay of the diffuse components, the power of the diffuse components at $\tau = \tau_d$, and the normalized coherence bandwidth of the diffuse components. The parameter vector $\Theta_{\text{smc}}^{\text{XY}}$ groups the parameters associated with the SMCs and includes the geometrical parameters defining each specular path, that is, the azimuth of departure/arrival, the elevation of departure/arrival, and time of arrival. These geometrical parameters are identical across all polarization sub channels. Further, $\Theta_{\text{smc}}^{\text{XY}}$ includes the complex amplitude γ^{XY}, that differ between different polarization due to the polarization-dependency of electromagnetic interactions (e.g. reflections, diffractions, diffusions, etc.).

The maximum likelihood estimator, RiMAX, [32, 33] is used for the joint estimation of the parameters $\Theta_{\text{smc}}^{\text{XY}}$ and Θ_{dmc}. For the collected data, the DMC parameters have been fully investigated [17]. Also, the large-scale parameters, such as the root-mean-square (rms) delay spread, the path loss, the XPD, the CPR, and so on, have also been determined [17]. Therefore, our main contribution is the investigation of the industrial multipath angular characteristics.

3.2 | Clustering of the multipath components

A cluster is a set of MPCs that have similar propagation characteristics. Several researches have shown that the MPCs arrive in clusters mode in industrial environments [12–15]. It is important to consider the multipath clustering in channel modelling; otherwise, the channel model overestimates the channel capacity [34].

The clustering of multipath depends on the delays, powers, and angles of arrival/departure. As our antenna system is a virtual UCA in the horizontal plan, we assume that the angles of elevation of MPCs are uniformly distributed [35], and the angles of azimuth are estimated from the measurement data. The estimated specular paths are grouped into clusters using the K-powers-means algorithm [36], and the multipath component distance (MCD) is used as a metric to distinguish the clusters. For path i and j ($i = j$), the MCD is determined in both the azimuthal and elevation AOA in Equation (7) and delay domains in Equation (8).

$$\text{MCD}_{\text{Angle}}^{\text{i, j}} = \frac{1}{2}|\mathbf{a}_i - \mathbf{a}_j| \tag{7}$$

with $\mathbf{a}_k = [\sin(\theta_k)\cos(\varphi_k), \cos(\theta_k)\cos(\varphi_k), \cos(\varphi_k)]^T$ where θ_k and φ_k designate the elevation and azimuth angle of the kth path, respectively.

$$\text{MCD}_{\text{Delay}}^{\text{i, j}} = \zeta \frac{|\tau_i - \tau_j|\tau_{std}}{\Delta\tau_{max}^2} \tag{8}$$

where τ_{std} is the standard deviation of the delays, $\Delta\tau_{max} = \max_{i,j}(|\tau_i - \tau_j|)$, and ζ is a suitable delay scaling factor fixing the importance of the delay domain. Here, we set $\zeta = 1$. The resulting metric to discriminate the clusters is as follows:

$$\text{MCD}_{\text{i, j}} = \sqrt{\text{MCD}_{\text{Angle}}^{\text{i,j}\ 2} + \text{MCD}_{\text{Delay}}^{\text{i,j}\ 2}} \tag{9}$$

The number of clusters N is iteratively determined according to the following heuristic [36]. First, the number of clusters is initialized to $N_c = 20$. Second, the K-powers-means algorithm is performed with N_c to identify clusters. If one (or more) estimated cluster power is less than a threshold, then $N_c = N_c - 1$ and the second step is executed again; otherwise, the number of clusters N equals N_c and this ends the heuristic. To avoid detection of insignificant clusters, the power of an identified cluster should be at least 1% of the total power.

4 | RESULTS

4.1 | Multipath estimation

The RiMAX algorithm [32] is used to extract the SMC parameters. For a given path k and polarization state XY, the considered parameters are the complex amplitude γ_k^{XY}, elevation of arrival $\theta_{\text{k}}^{\text{EoA}}$, azimuth of arrival $\varphi_{\text{k}}^{\text{AoA}}$, and delay τ_{k}. The power of the estimated SMCs has been normalized so that its maximum is 0 dB. Besides, the SMCs those relative powers at least of −50 dB are kept; otherwise, they are not considered because their contributions are too weak. We focus here on the angles of arrival as we are more interested in the locations of the Rx.

Figure 2 (resp. Figure 3) shows the scatter plots of the MPCs for the four polarizations for location 1 (resp. 20) in LOS (resp. OLOS) scenario. The colour bar indicates the path's relative power. Figure 2(a), (b), (c), and (d) consists of 139, 176, 143, and 131 paths, respectively, whereas Figure 3(a), (b), (c), and (d) consists of 84, 83, 84, and 83 paths, respectively. On an average, we obtain 119 paths and 72 paths for the LOS and OLOS scenarios, respectively. As it can clearly be seen in Figure 4, the number of MPCs in LOS condition is higher than in the OLOS. This is explained by the obstruction in the OLOS scenario where several MPCs do not reach the Rx because of their low SNR in contrary to the LOS where more MPCs are expected. The number of MPCs depend on the discriminatory power of the algorithm, the SNR, and the threshold criteria, and indicate the number of MPCs that were successfully extracted by RiMAX. In reality, there may be tens or hundreds of MPCs in the channel that could not be extracted because of the limitations of the algorithm, but the aforementioned trend in LOS and OLOS conditions will be the same.

Figure 5(a) and (b) show the probability density function (pdf) of the azimuth AoA for the LOS and OLOS scenarios, respectively. The azimuth is spread from 0° to 360°, indicating that the MPCs arrive in diffuse fashion as it as been observed in various works [20, 37, 27]. Besides, the investigation shows that the multipath arrive according to favourite directions in

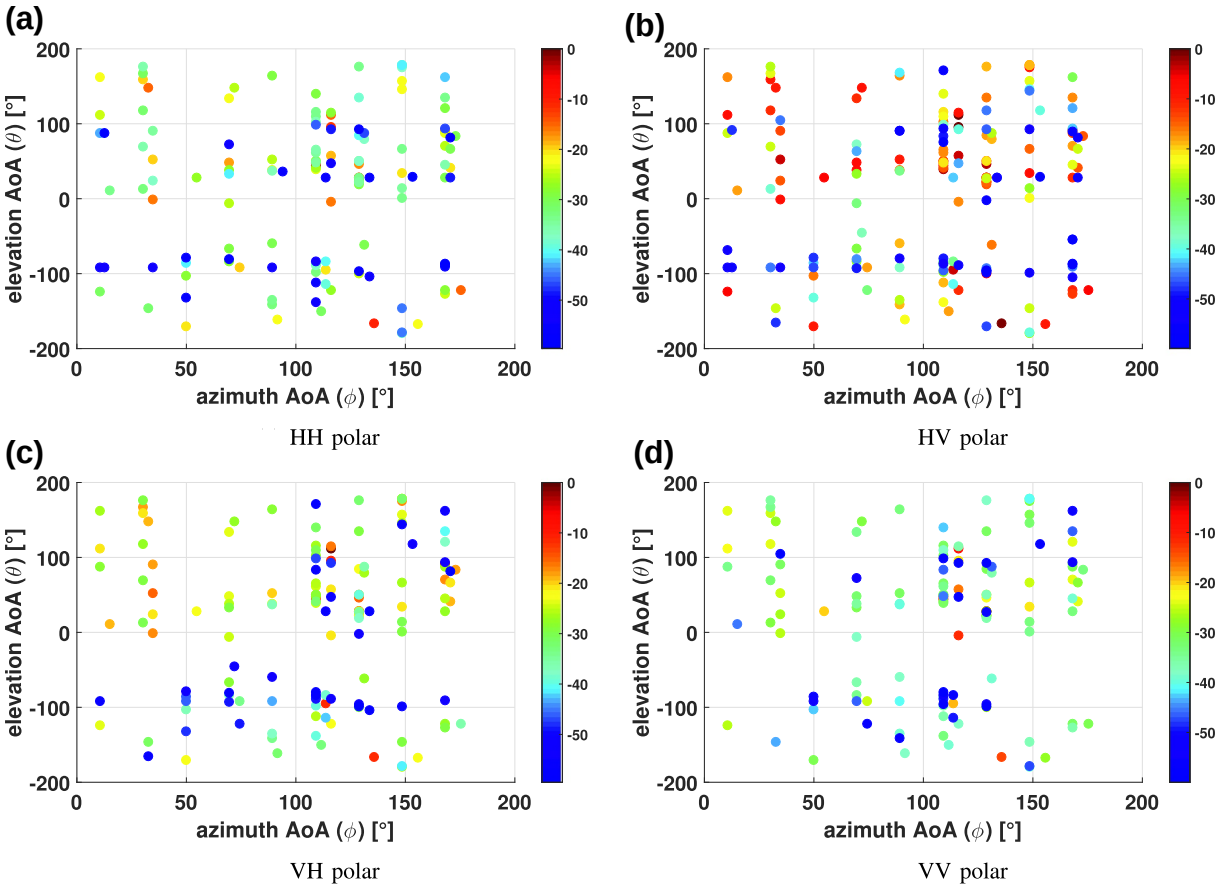

FIGURE 2 Multipath parameters at Position 1 (LOS conditions). LOS, line-of-sight

the azimuthal angle, irrespective of the scenarios and polarizations, that is, the majority of the paths arrive within [−100° −80°] and [80° 100°]. The pdf of the azimuth AoA in both the LOS and OLOS suggest clustering of the multipath as they look similar to a multimodal normal distribution [38]. As a matter of fact, the two pdf show clearly that the multipath can be classified into two groups, at least in the angular domain. We will therefore investigate the multipath clustering in the following section.

4.2 | Clustering results

Figures 6 and 7 show the clustering results of the MPCs at Position 1 (LOS) and Position 20 (OLOS), respectively. At these locations, a maximum of three clusters is observed, regardless of the polarization. The red circles, blue squares, and black triangles indicate the first, second, and third cluster, respectively. The yellow marker shows the centroid of the corresponding cluster. The number of clusters is determined using the heuristic described at the end of Section ¡def mbox : mbox ¡def ¡mbox :mbox mbox III-B¡mbox. It varies from 1 to 4 as indicated in Figure 8. The minimum and maximum number of cluster occur in OLOS and LOS conditions, respectively. This can be explained as follows. The OLOS scenario tends to block more multipath to arrive at the Rx as compared to the LOS. As we obtained similar distribution in both the LOS and OLOS conditions for the azimuth, it is clear that more (resp. less) MPCs will lead to more (resp. less) clusters. However, in either the LOS or OLOS case, three clusters have been obtained with the highest probability, as indicated in Figure 8. These findings agree with literature as four to six clusters (average value of 5) have been assessed in an industrial environment measurement from 3.1 to 10.6 GHz [12], whereas six to eight clusters (average value of 7) have been obtained in another industrial environment [13] measurements campaign from 800 MHz to 4 GHz. Both studies determined the clusters by visual inspection, hence in a more or less subjective manner. Although we identify the clusters in this study with an algorithm, the clustering result is somewhat eventually subjective because the number of multipath—hence the number of clusters—will depend on the dynamic measurement range. Obviously, the measured frequencies certainly have an impact on the number of clusters, that is, the number of clusters decreases with increasing frequencies [27].

The experiment further shows that the first cluster arrives always in the LOS (or OLOS) direction, and the following clusters stem from specular reflections on the walls, furniture, metallic structures, and so on surrounding the receiver.

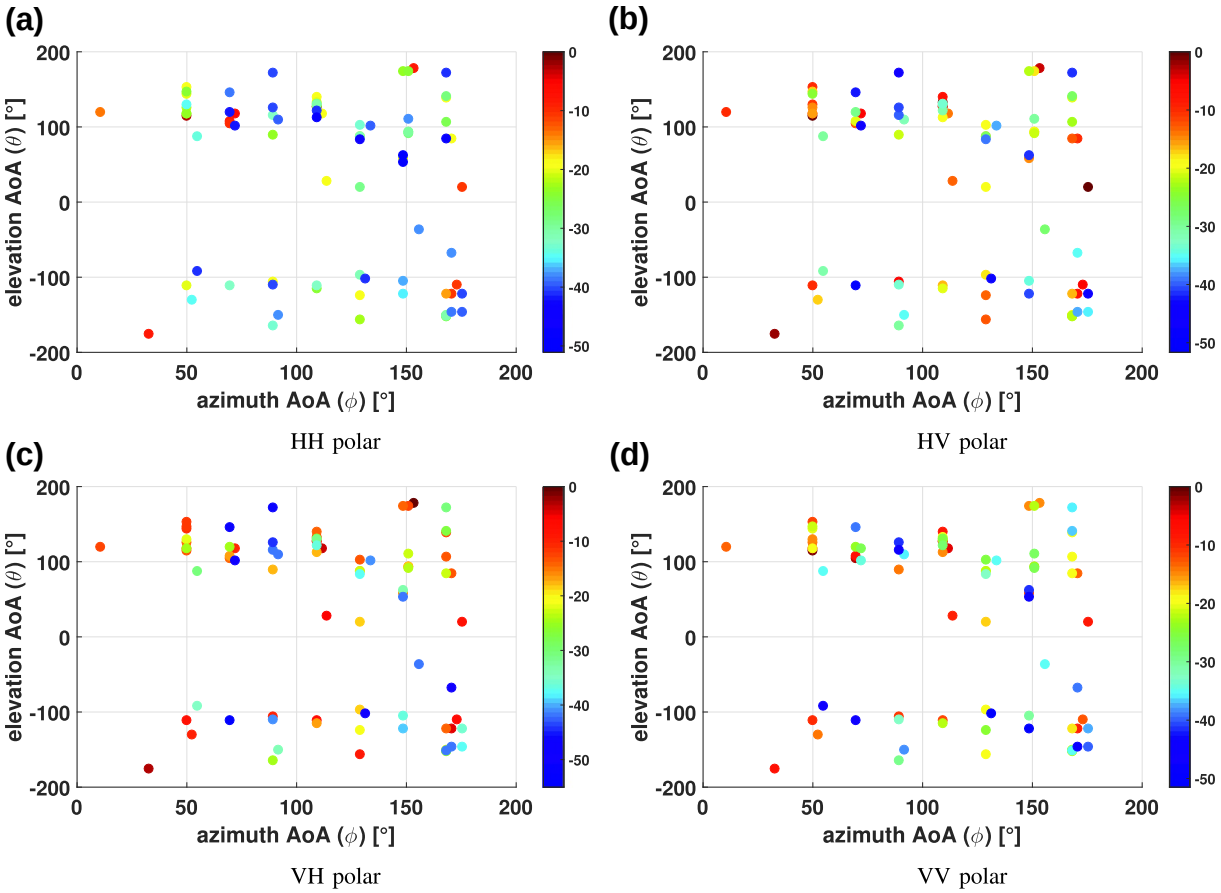

FIGURE 3 Multipath parameters at Position 20 (OLOS conditions). OLOS, obstructed line-of-sight

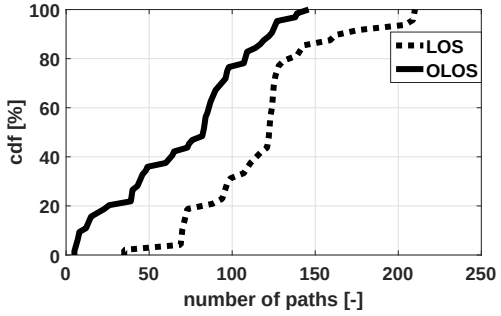

FIGURE 4 Cumulative distribution function of the number of paths for LOS and OLOS scenarios. LOS, line-of-sight; OLOS, obstructed line-of-sight

Moreover, we investigated the contribution of the first cluster in the total received power. Figure 9 shows the first's cluster contribution to the four polarization states. In general, we observe that the first clusters have the highest contribution in the total power, especially for the co-polarization HH and VV. The remainder clusters may have the highest contribution of received power, especially for the cross-polarization HV and VH. The cdf of the first's cluster contribution in the total power for the co-polar are similar, alike for the cross-polar. Also, we find that the first cluster contribution for the co-polarization is always higher than the one of the cross-polarization, as it can be seen in Figure 9.

4.3 | Intra-cluster large-scale parameters

The multipath clustering and associated properties such as the intra-cluster delay and angular dispersion are important features [34], especially for an efficient design of WSN in industrial environments. We determine the rms values in the delay and angular (i.e. azimuth) domains. The knowledge of the rms delay spread is important as it set the bit error or maximum achievable throughput of communications systems. The rms delay spread is also used to generate small-scale parameters such as the delays, clusters' powers for link-level, and system-level simulations of a new technology [39]. For a XY polarization, the rms delay spread of a cluster l is expressed as follows:

$$\sigma_{\mathrm{DS}}^{\mathrm{l,XY}} = \sqrt{\frac{\sum_{m=1}^{M_l} (\tau_{\mathrm{m}} - \overline{\tau}_{\mathrm{l}})^2 \alpha_{\mathrm{m}}^{\mathrm{XY}}}{\sum_{m=1}^{M_l} \alpha_{\mathrm{m}}^{\mathrm{XY}}}} \tag{10}$$

where $\overline{\tau}_{\mathrm{l}}$ is the mean arrival delay of the paths within the cluster l and is defined as follows:

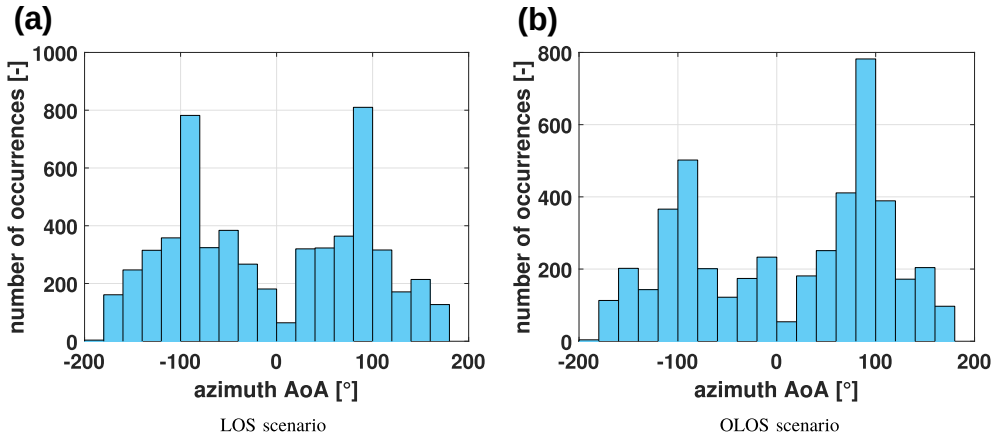

FIGURE 5 Probability density function of the azimuth AoA: (a) LOS scenario and (b) OLOS scenario. AOA, angle-of-arrival; LOS, line-of-sight; OLOS, obstructed line-of-sight

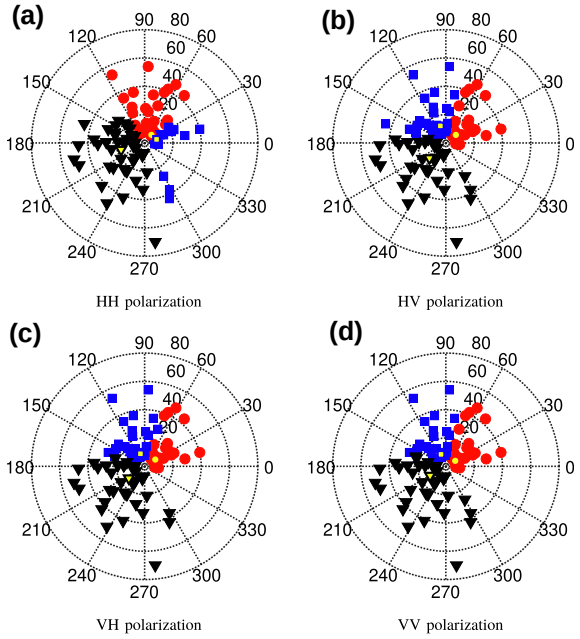

FIGURE 6 Multipath clustering at Position 1 (LOS conditions). The concentric circles indicate the paths travelled distances (in metres). LOS, line-of-sight

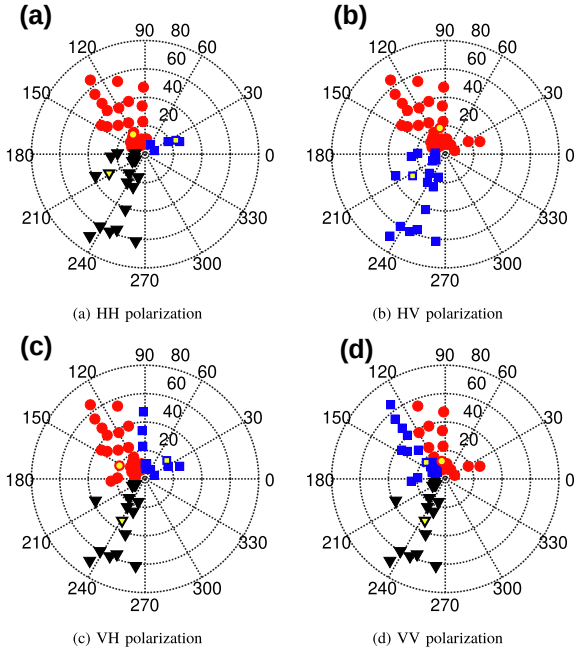

FIGURE 7 Multipath clustering at Position 20 (OLOS conditions). The concentric circles indicate the paths' travelled distances (in meters). OLOS, obstructed line-of-sight

$$\overline{\tau_l} = \frac{\sum_{m=1}^{M_l} \alpha_m^{XY} \tau_m}{\sum_{m=1}^{M_l} \alpha_m^{XY}} \tag{11}$$

M_l, $\alpha_m^{XY}=\gamma_m^{XY2}$, and τ_m are the number of paths in the cluster l, the power (for a XY polarization), and the arrival delay of the mth path within the cluster l, respectively.

Concerning the rms angular spread, it shows the extent of the space selectivity, and is related to the space correlation in multiple-input multiple-output (MIMO) antennas systems. The general definition of the rms angular spread provides values from 0 to 1 [40], and overcome the periodicity of the angles. According to that definition, a rms angular spread value of 0 indicates that the MPCs arrive (or depart) in a single direction, whereas a value of 1 indicates that there is no preference in the direction of arrival (or departure) of the MPCs. However, we adopt the definition of [41] (expressed in degrees) as it suits for small values of angular spread as expected for clusters; for an XY polarization, it is defined as follows.

$$\sigma_{ASA}^{l,XY} = \sqrt{\frac{\sum_{m=1}^{M_l} (\varphi_m - \overline{\varphi_l})^2 \alpha_m^{XY}}{\sum_{m=1}^{M_l} \alpha_m^{XY}}} \tag{12}$$

with φ_m is the azimuth AOA of the mth path in the cluster and $\overline{\varphi_l}$ is the mean arrival azimuth of the MPCs of a cluster l and is defined as follows:

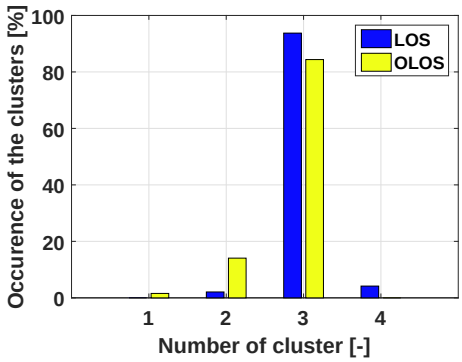

FIGURE 8 Probability density function of the number of clusters

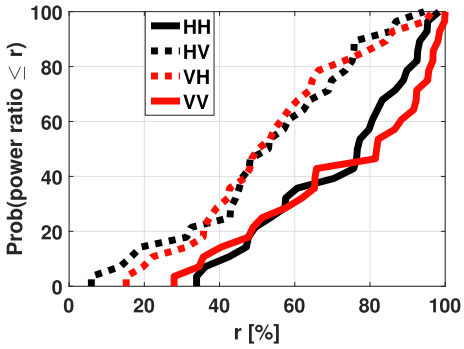

FIGURE 9 Cumulative distribution functions of the first cluster's contribution in the total power for polarization HH, HV, VH, and VV

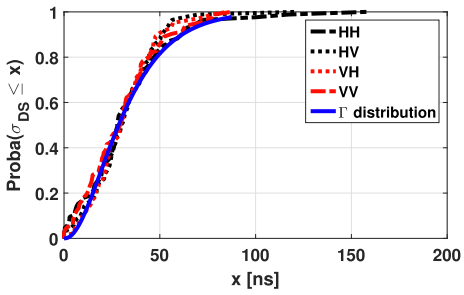

FIGURE 10 Cumulative distribution functions of the root mean square delay spread (σ_{DS})

$$\overline{\varphi_{\mathrm{l}}} = \frac{\sum_{m=1}^{M_l} \alpha_{\mathrm{m}}^{\mathrm{XY}} \varphi_{\mathrm{m}}}{\sum_{m=1}^{M_l} \alpha_{\mathrm{m}}^{\mathrm{XY}}} \tag{13}$$

The statistics of intra-cluster's rms delay spread ($\sigma_{\mathrm{DS}}^{\mathrm{l,XY}}$) and rms angular spread ($\sigma_{\mathrm{ASA}}^{\mathrm{l,XY}}$) are addressed. Figures 10 and 11 show respectively the cdf of the rms delay spread (σ_{DS}) and angular spread (σ_{ASA}) values for the different polarizations.

We observe that the rms delay spread, that is σ_{DS}—for all the polarizations HH, HV, VH, and VV—follow the same distribution (Figure 10). This observation is also the same for the rms angular spread, that is, σ_{ASA} as we see from Figure 11, the four cdf follow similar distribution. This tendency is confirmed by the Kolmogorov–Smirnov (KS) test. For the

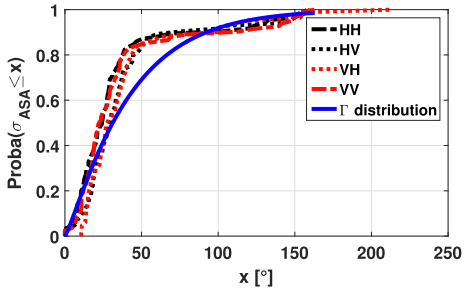

FIGURE 11 Cumulative distribution functions of the root mean square angular spread (σ_{ASA})

TABLE 1 Parameters of the gamma function

	a	*b*
$\sigma_{\mathrm{DS}}^{\mathrm{l,XY}}$	2.40	13.90
$\sigma_{\mathrm{ASA}}^{\mathrm{l,XY}}$	1.20	34.70

HH, HV, VH, and VV polarization, the KS test was respectively performed with 85, 84, 83, and 82 samples (corresponding to the total number of clusters) for both σ_{DS} and σ_{ASA} with the default p-value of 0.05 for which the null hypothesis is accepted. In fact, the KS test confirms that the σ_{DS} values for the four polarization states follow the same distribution, alike for the σ_{ASA}. Furthermore, we have compared several probability distributions to the empirical cdf of the σ_{DS} and σ_{ASA}, and it turns out that the gamma distribution is the one that suits them the best. In Figure 10 (resp. Figure 11), the solid blue line is the gamma distribution that suits best the distribution of $\sigma_{\mathrm{DS}}^{\mathrm{l,XY}}$ (resp. $\sigma_{\mathrm{ASA}}^{\mathrm{l,XY}}$) for all polarizations.

Hence, for a given polarization XY, the following distribution is considered for $\sigma_{\mathrm{DS}}^{\mathrm{l,XY}}/\sigma_{\mathrm{ASA}}^{\mathrm{l,XY}}$:

$$\mathrm{pdf}(x;a,b) = \frac{x^{a-1}e^{-\frac{x}{b}}}{\Gamma(a)b^a}, \qquad \text{for} \quad x>0, \quad \text{and} \quad a,b>0 \tag{14}$$

where $\Gamma(.)$ is the gamma function and the parameters a and b are defined in Table 1. Obviously, the gamma distribution parameters (i.e. a and b) may vary for different environments. Similar distributions have been observed in [27] for the rms angular spread in an office and conference room at millimeter-wave frequencies.

5 | CONCLUSION

This study provides a comprehensive characterization of the multipath in the angular domain. The characterization focuses on the specular paths in an indoor industrial environment in both LOS and OLOS scenarios, although the presence of strong diffuse scattering has been evidenced. The full polarimetric channel is considered, and the multipath parameters are assessed by means of a maximum likelihood estimator. The

investigated indoor industrial environment is very rich in multipath, for example, several tens, more than in offices or conference rooms. This is caused by the multiple reflectors and machinery around the transceivers. Additionally, it turns out that the number of multipath in LOS scenario is about two times of that found in NLOS case. Moreover, the assessment shows that the MPCs arrive in clusters, irrespective of the polarization and propagation scenario. We obtain one to four clusters, and the maximum number of cluster occurs for the LOS scenario. It is observed that the first cluster carries the majority of the power, and the trend is prominent for the co-polar in comparison to the cross-polar. Explicitly, the first cluster carries on average about 55% and 80% of the total power for the cross-polarization and co-polarization, respectively. The statistics of the intra-clusters parameters have also been addressed. It is found that both the rms delay spread and rms angular spread follow a gamma distribution, and that is independent of the polarization states. In general, we observe that the polarization and propagation conditions have very little impact on the multipath characteristics in the angular domain; but, the environment itself, including the density and configuration of the scatterers and obstacles, have an impact thereon. Our findings agree well with those found in the literature review.

The modelling of the multipath propagation in the delay, elevation, and azimuth domains in such environments will be part of our future study.

ORCID

Aliou Bamba https://orcid.org/0000-0002-2144-7085
Davy P. Gaillot https://orcid.org/0000-0003-3455-5824

REFERENCES

1. Rappaport, T.S.: Indoor radio communications for factories of the future. IEEE Commun. Mag. 27(5), 15–24 (1989)
2. US Department of Energy: Industrial wireless technology for the 21st century. Off. Energy Renew. Energy Rep. (2002)
3. Gungor, V.C., Lambert, F.C.: A survey on communication networks for electric system automation. Comput. Netw. 50(7), 877–897 (2006)
4. Gungor, V.C., Hancke, G.P.: Industrial wireless sensor networks: challenges, design principles, and technical approaches. IEEE Trans. Ind. Electron. 56(10), 4258–4265 (2009)
5. Dahlman, E., et al.: 5G NR: The Next Generation Wireless Access Technology. Academic Press (2018)
6. Kukushkin, A.: Introduction to Mobile Network Engineering: GSM, 3G-WCDMA, LTE and the Road to 5G. John Wiley & Sons Ltd (2018)
7. Hampicke, D., et al.: Characterization of the directional mobile radio channel in industrial scenarios, based on wide-band propagation measurements. In: IEEE vehicular technology conference (VTC), 2258–2262.IEEE, Amsterdam, Netherlands (1999).
8. Candell, R.: A research framework for industrial wireless deployments. In: Proceedings of 2015 ISA instrumentation symposium, Huntsville (2015)
9. Birdwell, J.D., et al.: Propagation modeling in a manufacturing environment. In Workshop on wireless communication for improved manufacturing, Oak Ridge, TN, 1–17 (1995)
10. Candell, R., et al.: Industrial Wireless Systems Radio Propagation Measurements. National Institute of Standards and Technology, U.S. Department of Commerce Gaithersburg, MD (2017)
11. Wassie, D.A., et al.: Radio propagation analysis of industrial scenarios within the context of ultra-reliable communication. In IEEE 87th vehicular technology conference (VTC Spring), 1–6, Porto, Portugal (2018)
12. Karedal, J., et al.: A measurement-based statistical model for industrial ultra-wideband channels. IEEE Trans. Wireless Commun. 6(8), 3028–3037 (2007)
13. Tanghe, E., et al.: The industrial indoor channel: statistical analysis of the power delay profile. Int. J. Electron. Commun. 64(9), 806–812 (2010)
14. Ferrer-Coll, J., et al.: Characterisation of highly absorbent and highly reflective radio wave propagation environments in industrial Applications. IET Commun. 6(15), 2404–2412 (2012)
15. Ferrer Coll, J.: Channel Characterization and Wireless Communication Performance in Industrial Environments. PhD thesis. University of Gävle (Stockholm - Sweden), Faculty of Engineering and Sustainable Development, Department of Electronics, Mathematics and Natural Sciences, Electronics. KTH, Radio Systems Laboratory (RS Lab)., Stockholm (2014)
16. Saleh, A.A.M., Valenzuela, R.A.: A statistical model for indoor multipath propagation. IEEE J. Sel. Areas Commun. 5(2), 128–137 (1987)
17. Gaillot, D.P., et al.: Polarization properties of specular and dense multipath components in a large industrial hall. IEEE Trans. Antennas Propag. 63(7), 3219–3228 (2015)
18. Ramanathan, R.: On the performance of ad hoc networks with beamforming antennas. In Proceedings of the 2nd ACM international symposium on mobile ad hoc networking and computing, ACM Press, Long Beach, CA, 95–105, (2001)
19. Anderson, E., et al.: The impact of directional antenna models on simulation accuracy. In: 7th international symposium on modeling and optimization in mobile, ad hoc, and wireless networks (WiOpt), Seoul, Korea (South) (2009)
20. Anderson, E., et al.: Modeling environmental effects on directionality in wireless networks. Math. Comput. Model. 53, 2078–2092 (2011)
21. Gurrieri, L.E., et al.: Characterization of the angle, delay and polarization of multipath signals for indoor environments. IEEE Trans. Antennas Propag. 56(8), 2710–2719 (2008)
22. Kim, M., et al.: Large scale parameters and double-directional characterization of indoor wideband radio multipath channels at 11 GHz. IEEE Trans. Antennas Propag. 62(1), 430–441 (2014)
23. Zhang, N., et al.: Measurement-based angular characterization for 72 GHz propagation channels in indoor environments. In: IEEE Globecom workshops (GC Wkshps), IEEE, Austin, TX, (2014)
24. Gustafson, C., et al.: On mm-wave multipath clustering and channel modeling. IEEE Trans. Antennas Propag. 62(3), 1445–1455 (2014)
25. Kim, M.-D., et al.: Directional delay spread characteristics based on indoor channel measurements at 28 GHz. In IEEE 26thannual international symposium on personal, indoor, and mobile radio communications (PIMRC), IEEE, Hong Kong, China (2015)
26. Medbo, J., et al.: Frequency dependency of measured highly resolved directional propagation channel characteristics. In 22th European wireless conference, Oulu, Finland. European Wireless, 2016
27. Bamba, A., et al.: Millimeter-wave indoor channel characteristics in V and E bands. IEEE Trans. Antennas Propag. 66(10), 5409–5424 (2018)
28. Zhang, G., et al.: Experimental characterization of millimeter-wave indoor propagation channels at 28 GHz. IEEE Access. 6, 76516–76526 (2018)
29. Pometcu, L., D'Errico, R.: An indoor channel model for high data-rate communications in D-band. IEEE Access. 8, 9420–9433 (2019)
30. Miaoudakis, A., et al.: Radio channel characterization in industrial environments and spread spectrum modem performance. In: IEEE conference on emerging technologies and factory automation. IEEE, Catania, Italy (2005)
31. Ai, Y., et al.: Geometry-based modeling of wideband industrial indoor radio propagation channels. In: 41st annual conference of the IEEE industrial electronics society (IECON), Yokohama, Japan (2015)
32. Richter, A.: Estimation of Radio Channel Parameters: Models and Algorithms. PhD thesis. Faculy of Electrical Engineering and Information Technology - Technical University Ilmenau, Germany (2005)
33. Richter, A., Thoma, R.S.: Joint maximum likelihood estimation of specular paths and distributed diffuse scattering. In IEEE 61st vehicular technology conference, IEEE, Stockholm, Sweden, 1, 11–15, 2005
34. Li, K.H., et al.: Impact of clustering in statistical indoor propagation models on link capacity. IEEE Trans. Commun. 50(4), 521–523 (2002)

35. Shafi, M., et al.: The impact of elevation angle on MIMO cCapacity. In: IEEE international conference on communications, Istanbul, Turkey. IEEE (2006)
36. Czink, N.: The Random Cluster Model – A Stochastic MIMO Channel Model for Broadband Wireless Communication Systems of the 3rd Generation and Beyond. PhD thesis. Technischen Universität Wien (2007)
37. Virk, U.T., et al.: Multi-frequency power angular spectrum comparison for an indoor environment. In: 11th European conference on antennas and propagation (EUCAP). IEEE, Paris, France (2017)
38. Baudry, J.P., et al.: Combining mixture components for clustering. J. Comput. Graph. Stat. 19(2), 332–353 (2010)
39. 3GPP TR 38.901: 3rd Generation Partnership Project; Technical Specification Group Radio Access Network; Study on channel model for frequencies from 0.5 to 100 GHz (Release 14). Tech. Rep. v14.0.0 (2017)
40. Fleury, B.H.: First- and second-order characterization of direction dispersion and space selectivity in the radio channel. IEEE Trans. Inf. Theory. 46(6), 2027–2044 (2000)
41. Czink, N., et al.: Cluster angular spreads in a MIMO indoor propagation environment. In: IEEE 16th international symposium on personal, indoor and mobile radio communications (PIMRC), 664–668, Berlin, Germany, (11–14 September 2005)

How to cite this article: Bamba A, Tanghe E, Kamagaté A, et al. Angular characteristics of multipath propagation in an indoor industrial environment. *IET Microw. Antennas Propag.* 2021;15:768–777. https://doi.org/10.1049/mia2.12082